Astron. & Astrophys. 38, 381—390 (1975)

The Structure of the Radio Galaxy NGC 1265

G. K. Miley
Sterrewacht, Leiden

K. J. Wellington
Radiosterrewacht, Dwingeloo

H. van der Laan
Sterrewacht, Leiden

Received October 31, 1974

Summary. New data are presented on the 5 GHz polarization distribution of the head tail radio galaxy NGC 1265 in the Perseus Cluster. A comparison with previously reported Westerbork measurements at 1.4 GHz has yielded information about the distributions of spectral index, magnetic field direction and rotation measure in the source. The reduction procedure and various uncertainties are discussed at length. The magnetic field vectors are well aligned along the tail and the percentage polarization reaches 60% in places indicating that magnetic energy is dominant. In addition there appears to be a gradient in rotation measure across the tail. These results are in agreement with the predictions of the magnetospheric trail model for head tail radio sources. The physical conditions inside and outside the source are discussed within the framework of several assumptions. Our derived magnetic field strengths (~ 3–$7\,\mu$G), electron densities ($\sim 10^{-3}$ to $10^{-4}\,\mathrm{cm}^{-3}$) and temperatures ($\sim 10^{7}$ K) are similar to those previously reported for 3C129.

Key words: radio sources — galaxies — clusters — polarization — magnetic fields — intergalactic matter

1. Introduction

The radio emission from the galaxy NGC 1265 in the Perseus Cluster has been the subject of extensive investigation (Ryle and Windram, 1968; Hill and Longair, 1971; Miley *et al.*, 1972; Riley, 1973; Miley, 1973; Wellington *et al.*, 1973). This source, 3C 83.1B, has a distinctive head-tail morphology. A summary of the properties of head tail radio sources has been given by Miley *et al.* (1973) who point out the various analogies with double radio galaxies.

The most satisfactory explanation of these tadpole-shaped sources is the "radio trail" hypothesis (Miley *et al.*, 1972). The tail is explained as a remnant left behind when an active radio galaxy hurtles through the cluster medium. More detailed radio trail models have been discussed by Jaffe and Perola (1973). It is clear that a study of these sources can give unique insight into the properties of cluster and the evolution of radio sources. In this article we present total intensity and polarization data on NGC 1265 obtained with the Westerbork Synthesis Radio Telescope (WSRT) (Högbom and Brouw, 1974; Baars *et al.*, 1973) at frequencies of 1415 and 4995 MHz. These give new information about the properties of the source. In particular, we obtain a detailed picture of the geometry of the magnetic field which can be related to the magnetospheric model of Jaffe and Perola.

2. Observations and Reductions

The 1.4 GHz observations have been described by Miley (1973) and the 5 GHz observations by Wellington *et al.* (1973). Table 1 gives the relevant parameters. For both cases eighty contiguous baselines were used ranging in length from 36 m to 1458 m in steps of 18 m. Four correlators are attached to each baseline of the WSRT. Their outputs, after Fourier transformation and linear combination, give maps of the four Stokes parameters (Weiler, 1973) over a region defined by the beam of the 25 m primary dishes.

At 5 GHz the 11′ primary beam is comparable with the overall source size. To obtain maximum information about the low brightness regions of the source the 5 GHz observations were therefore carried out with the field centred about halfway along the tail.

The standard WSRT calibration procedure was used. Fringe amplitudes were referred to 3C 147, assumed

Table 1. Parameters of the observations and reduction for NGC 1265

Observing period	1971.5–1971.8		1973.0–1973.3		
Frequency (MHz)	1415		4995		
Bandwidth (MHz)	4.2		4.2		
Primary beam and field centre (RA/dec., 1950)	$03^h15^m/41°38'$		$03^h15^m/41°45'$		
Half-power diam. of primary beam	36′		11′		
Baseline increment	18 m (85 λ)		18 m (300 λ)		
Radius of first grating ring (in RA)	49′		14′		
Map computed	*A*	*B*	*A*	*B*	*C*
Shortest spacing	36 m (170 λ)	126 m (595 λ)	36 m (600 λ)	36 m (600 λ)	36 m (600 λ)
Longest spacing	1458 m (6883 λ)	1458 m (6883 λ)	414 m (6899 λ)	1458 m (24296 λ)	1458 m (24296 λ)
Spacing with 25 % taper	1458 m (6883 λ)	1458 m (6883 λ)	413 m (6883 λ)	724 m (12065 λ)	1458 m (24296 λ)
Half-power diam. of synthesized beam (in RA)	23″	23″	23″	11″	6″
Separation of grid points	9″	9″	9″	2.″8	2.″8
Effective *rms* noise per synthesized beam at field centre (m.f.u.)[a]	0.6	0.6	1.0	0.8	0.6

[a]) One milliflux unit (m.f.u.) $= 10^{-29}\,\mathrm{Wm^{-2}Hz^{-1}}$.

unpolarized with flux densities of 21.57 f.u. at 1.4 GHz and 8.18 f.u. at 5 GHz. For the 1.4 GHz observations an additional calibrator was 3C 48, also assumed unpolarized with a flux density of 15.67 f.u.

The effective resolution of a synthesized map depends both on the baselines used and the grading function applied to the data before transformation. Several sets of maps were produced having the various baseline coverages and Gaussian tapers outlined in the lower part of Table 1. Maps at 5 GHz with resolutions of 6″, 11″ and 23″ allowed structure on a variety of scales to be investigated. The 23″ maps, when compared with 1.4 GHz maps of similar resolution, were used to derive spectral information about the total intensity and polarization distributions.

For the spectral work one needs maps at different frequencies which have as closely as possible the same grading function and baseline coverage. Although the baseline increment was 18 m, no data were available from the zero or 18 m baselines due to the finite size of the primary dishes. This problem of the "missing spacings" increases the difficulty of making exact comparison between maps at the two frequencies. As described by Miley (1973) the missing zero spacing introduces a constant negative offset in the map; the missing 18 m spacing has the effect of convolving the map with a first order Bessel function, thereby producing a variable offset on the same angular scale as the first grating ring. The magnitudes of both these effects depend on the strength and distribution of the brightness in the field. For the convolved 5 GHz maps, the missing spacings comprise relatively the largest number of baselines and here their absence is the most detrimental amongst our set of maps. To investigate this effect, two sets of 1.4 GHz maps were computed. The first set *A* was standard, including all available spacings, whereas the second *B* discarded all spacings shorter than 126 m. The 1.4 GHz *B* maps have a baseline coverage comparable with the 5 GHz *A* maps. A comparison of the 1.4 GHz *A* and *B* sets should allow us to estimate empirically the importance of the missing spacings for the 5 GHz 23″ maps.

3. Results and Errors

3.1. Intensity Spectra

Figure 1 shows the variation of spectral index along the tail. The high frequency indices $\alpha(1.4, 5.0)$ were obtained by comparing the 1.4 GHz *B* and 5 GHz *A* maps. Effects due to the missing spacings were minimized by estimating the brightness and local map-zeros from intensity profiles drawn through the tail. The data were then corrected for the primary beam response patterns.

The main sources of error in $\alpha(1.4, 5.0)$ are as follows:

(a) Effects of noise (see Table 1).

(b) Inaccurate zero level due to the missing spacings. The comparison of intensities from the 1.4 GHz *A* and *B* maps indicates that this is approximately $10\% \pm 5$ m.f.u.

(c) Uncertainties in the primary beam due to telescope mispointing. The present pointing accuracy at this declination is ~ 1 arc min. The resultant uncertainty in the primary beam correction increases with distance from the field centre, amounting at 5′ to $\pm 20\%$ for 5 GHz and to $\pm 4\%$ for 1.4 GHz.

(d) Errors in calibration ($\sim 5\%$).

Of course, except for the noise, all the above effects are correlated from point to point so that the error bars in the figure are not independent.

Figure 1 also shows the low frequency spectral indices $\alpha(0.4, 1.4)$ calculated in a similar way to $\alpha(1.4, 5.0)$ and taken from Miley (1973). Although no significant variation along the tail is apparent in $\alpha(0.4, 1.4)$, the high frequency spectra for both the east and west ridges steepen appreciably with distance from the galaxy. Riley (1973) did not find such an effect for 3C 83.1B (NGC 1265) in the Cambridge data but the highest frequency in her study was 2.7 GHz. The behaviour of $\alpha(1.4, 5.0)$ resembles that of $\alpha(0.4, 1.4)$ for the similar head tail source 3C 129 (Miley, 1973).

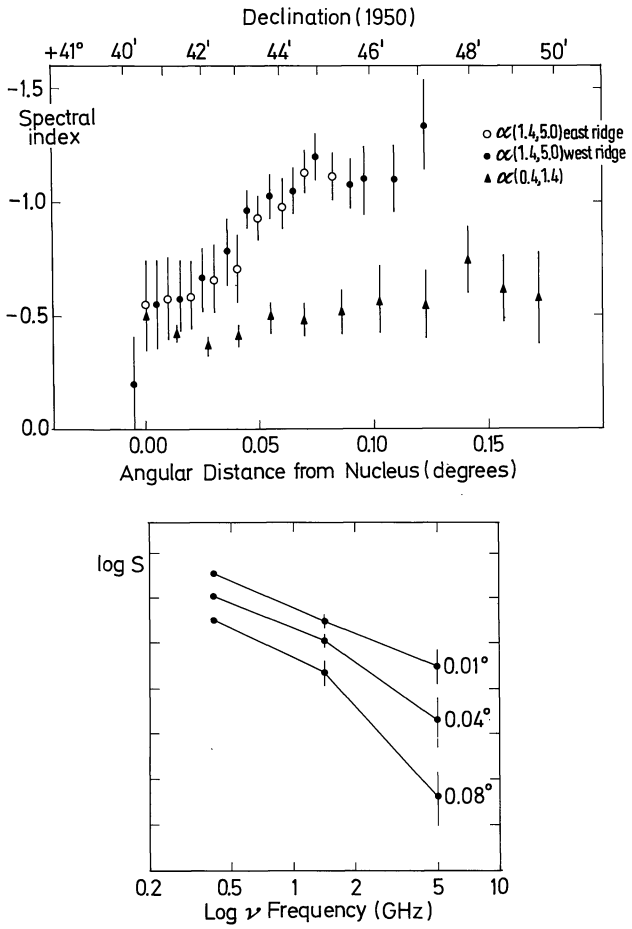

Fig. 1. (a) Variation of spectral index along the tail of NGC 1265. Low frequency indices are taken from the comparison of 408 MHz and 1415 MHz data by Miley (1973) (78″ resolution). High frequency values were derived from the 1.4 GHz and 5 GHz *A* maps (23″ resolution). Note that the error bars are not independent. (b) Relative spectra at some points along the tail of NGC 1265. Note that the low and high frequency parts have been obtained using maps with different resolution

However, since $\alpha(0.4, 1.4)$ refers to structure on a scale of 78″ and $\alpha(1.4, 5.0)$ to a scale of 23″, care must be taken in the interpretation of Fig. 1.

3.2. Polarization Data

Figure 2 shows the 5 GHz *C* map of the total intensity with a resolution of 6″ (Wellington *et al.*, 1973). The comparable polarization map is noise limited but significant polarization was detected from six points at the head. These are marked on the map together with the polarization directions. The percentage polarizations together with their estimated uncertainties are listed in Table 2.

The 5 GHz *B* map, with 11″ resolution, confirms these polarization peaks and shows some additional features in the head but does not have sufficient sensitivity to detect appreciable polarization in the tail. However, convolution of the 5 GHz data to 23″ resulted in detectable polarization over most of the source. Figure 3 gives the vector polarized intensities $\{P=(Q^2+U^2)^{\frac{1}{2}} \exp(i/2 \tan^{-1} U/Q)\}$ for the 5 GHz *A* and 1.4 GHz *B* maps. Vectors are plotted at every grid point where the signal is larger than 3σ. Since there are ~ 10 points per beam area, adjacent vectors are not independent.

The 23″ polarization maps are subject to the following errors:

(a) Effects of noise (see Table 1).

(b) Effects of missing spacings. Because the polarized intensities in the field at both frequencies are relatively low, the effect of the missing spacings will be much smaller in the polarization map than in the total intensity ones. This is confirmed by the fact that there is little difference between the 1.4 GHz *A* and *B* vector polarization maps. For the points plotted (~ 500), only a few were found to differ in position angle by more than 10°. Most of the position angles agreed to better than 5° and magnitudes to better than 10%.

(c) Uncertainties in the primary beam correction. Measurements on calibration sources indicate that this introduces an error of less than 2% in the polarized intensities at 5 GHz and 1% at 1.4 GHz (Weiler and Wilson, 1973).

(d) Errors in calibration ($\sim 5\%$ of polarized intensity).

(e) Instrumental polarization ($\sim 0.5\%$ of total intensity) (Weiler, 1973).

(f) Sidelobe distortion ($\sim 5\%$ of polarized intensity close to brightest peaks).

No circular polarization was detected on any of the maps. This was not unexpected and provides a partial check on the above estimation of errors.

4. Derivation of the Rotation Measure and the Magnetic Field

The remarkably smooth distribution of polarization angles shown in Fig. 3 indicates the presence of a magnetic field in NGC 1265 that is uniform over distances of several hundred kiloparsecs. The direction of the magnetic field as projected on the sky is perpendicular to that of the intrinsic electric vector. In general however, the directions of the observed and intrinsic electric vectors will differ due to Faraday rotation by the intervening magneto-ionic medium.

The polarization directions γ_λ, at a wavelength λ, are related to the intrinsic directions γ_0 by

$$\gamma_\lambda = \gamma_0 + R\lambda^2 .$$

The rotation measure is $R \propto n_e \boldsymbol{H} \cdot \boldsymbol{dl}$, where n_e is the free electron density and $\boldsymbol{H}$ is the magnetic field. Values of γ_λ at two different wavelengths, say γ_1 and γ_2 (at 6 cm and 21 cm in this case), in principle give γ_0 and R. However any measurement of γ_λ is subject to ambi-

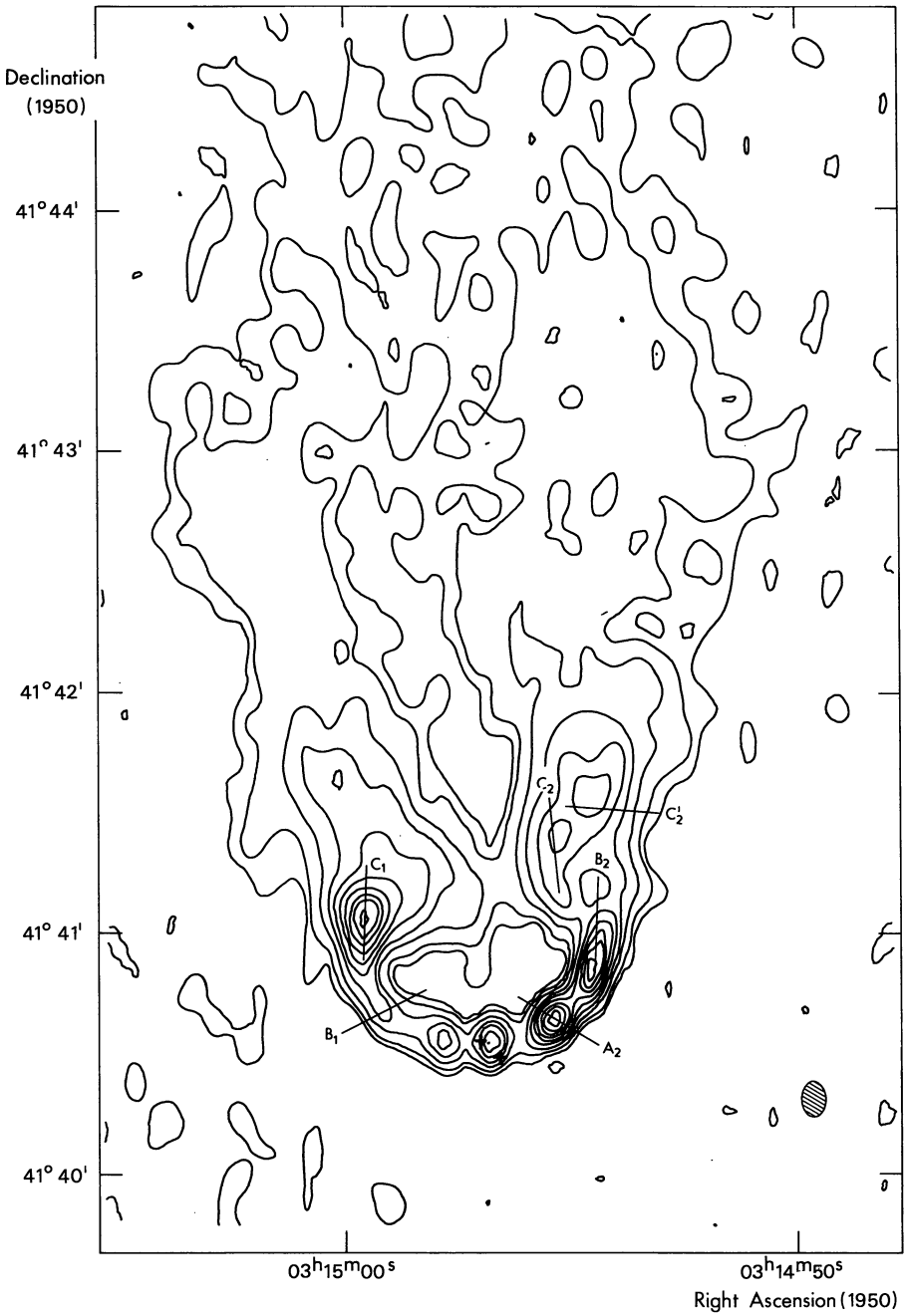

Fig. 2. The total intensity distribution in the head of NGC 1265 with a resolution of 6″. Contours are plotted at intervals of 2.5 m.f.u. per synthesized beam from 2.5 to 22.5 m.f.u. Also shown is the 1.25 m.f.u. contour. Equal length vectors mark the directions of points with significant polarization (see Table 2). The crosses mark positions for the nucleus of the galaxy measured independently by Heidmann (1973) and Tifft (1973). Here and in later figures the data are uncorrected for primary beam attenuation and the shaded ellipse represents the half-power synthesized beam

Table 2. 5 GHz polarizations of components in the head

Positions (see Fig. 2)	Percentage	Position angle (degree)
A_2	16 ± 8	60 ± 14
B_1	30 ± 15	118 ± 14
B_2	30 ± 15	179 ± 14
C_1	20 ± 8	178 ± 11
C_2	30 ± 10	6 ± 10
C_2'	24 ± 12	86 ± 14

guities of multiples of π. The measured rotation between wavelengths λ_1 and λ_2 is $\Delta\gamma = \gamma_2 - \gamma_1$.

Thus $R = \dfrac{\Delta\gamma + n\pi}{(\lambda_2^2 - \lambda_1^2)}$ where n is an integer.

Without measurements at further wavelengths or additional assumptions, it is not possible to derive the sign or value of R.

In our derivation of the magnetic field directions we shall assume that n is zero or -1, i.e. that -76 rad m^{-2}

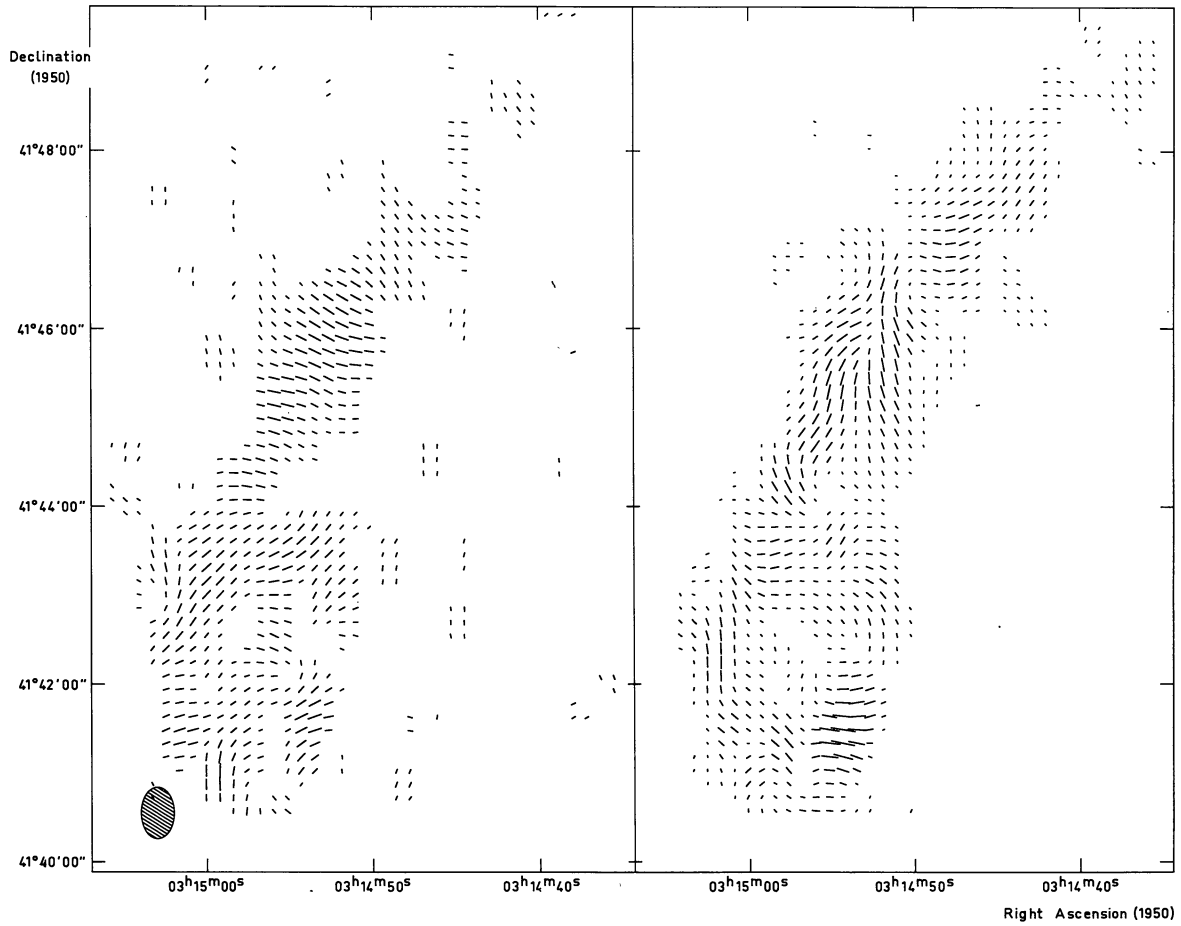

Fig. 3. Vector polarized intensities at 5 GHz (left) and 1.4 GHz (right), both with a 23″ resolution. 10 points are plotted per beam area and only points where the polarized intensity is larger than 2.5 m.f.u. are included

$< R \leqq +76\,\mathrm{rad\,m^{-2}}$. There are good grounds for the assumption that the foreground contributions to the rotation measure of NGC 1265 are not larger. First, the rotation measures of several nearby sources are smaller than $50\,\mathrm{rad\,m^{-2}}$ (Vallée and Kronberg, in preparation). Secondly, the rotation measure of NGC 1275 (3 C 84), dominant member of the Perseus Cluster and half a degree away, is given as $+55 \pm 10\,\mathrm{rad\,m^{-2}}$ (Mitton, 1972). Regarding the contribution of the source itself, the smoothness of observed 1.4 GHz polarization distribution and the slow variation of $\Delta\gamma$ over the source both argue for small rotation measures.

For every grid point with appreciable polarizations ($\geqq 4\sigma$) at both 1.4 and 5 GHz two values of the rotation measure were calculated using the above equation. The first (positive one) corresponded to $n=0$ and the second to $n=-1$, i.e. anticlockwise and clockwise rotation respectively. In this way a pair of rotation measures was derived for each grid point, differing by $76\,\mathrm{rad\,m^{-2}}$. For the anticlockwise and clockwise cases the mean rotation measure over the source was found to be $+44\,\mathrm{rad\,m^{-2}}$ and $-32\,\mathrm{rad\,m^{-2}}$ respectively. The positive value is comparable to the rotation measure of NGC 1275 cited above. Using these two sets of rotation measures and the polarization vectors in Fig. 3, pairs of intrinsic electric vectors and magnetic field directions were derived. The two sets of magnetic field vectors, differing by 16°, are plotted in Fig. 4. These diagrams show our best estimates for the *projected* magnetic field directions in NGC 1265.

The rotation measure sets can also be used to give information about the sign of the magnetic field component *along the line of sight*. To do this, the difference of the rotation measure of each point from the mean over the source was calculated and plotted in Fig. 5. This differential plot is clearly independent of the choice of the constant part of the rotation measure but is not necessarily solely due to contributions intrinsic to the source. For example the angular extent of more than 10′ and the eccentric location of NGC 1265 in the Perseus Cluster suggest that the contribution of the cluster to the foreground rotation measure may not be uniform.

The reduction procedure described above is shown in schematic form in Fig. 6.

5. Geometry of the Magnetic Field

The model for the formation of sources with radio tails which has been shown to best fit the observations

Fig. 4. The direction of the projected magnetic field in NGC 1265 assuming positive (left) and negative (right) values for the foreground rotation (see text). The white bars representing the field vectors are superimposed on a radio photograph of the 1.4 GHz intensity distribution

of the head-tail radio source 3 C 129 is the magnetospheric model by Jaffe and Perola (1973). In this model the parent galaxy possesses a dipole magnetic field which is dragged behind by the intergalactic medium as the galaxy moves through the cluster. This trailing magnetic field is illuminated from the galaxy by intermittent twin outbursts of relativistic particles, thereby forming a double radio tail. The authors drew an analogy between this phenomenon and the geomagnetospheric tail of the earth.

This simple magnetospheric model makes two clear predictions about the geometry of the magnetic field. First, the field lines should be *parallel* to the direction of motion of the galaxy. Secondly, the field lines in each tube of the double tail should derive from opposite poles of the galaxy's magnetosphere.

Both magnetic field distributions shown in Fig. 4 conform well to the first prediction. Of the two alternatives, the vectors in Fig. 4a appear slightly better aligned along the tail than those in Fig. 4b. In addition, the similarity between the mean rotation measure used in producing Fig. 4a and that of 3 C 84 (NGC 1275) leads us to prefer a constant foreground component of rotation that is anticlockwise.

A consequence of the second prediction is that the polarity of the magnetic field (and consequently the sign of the intrinsic rotation measure) should reverse *across* the tail. Now study the map of differential rotation measure in Fig. 5. The values are predominantly positive in the west and negative in the east part of the tail, in agreement with this prediction. However, because of the assumptions and uncertainties inherent in Fig. 5 (see Section 4), we cannot claim our rotation measure distribution to be more than marginal evidence in favour of the magnetospheric model.

The extreme polarization, up to 60 % in places (see Fig. 5 and Table 3), and remarkable uniformity of the magnetic field directions are both consistent with the simple picture of a one-dimensional field formed by dynamic stretching of a magnetic dipole. Since the field in the tail appears to have no significant fine structure on the kiloparsec scale or smaller, magnetic energy is probably dominant over particle energy.

There is an apparent constriction in the magnetic field vectors near declination 41°46′. Figure 5 shows a pronounced minimum of 1.4 GHz polarized intensity at the constriction, as well as a discontinuity in the behaviour of the rotation measure. A contour display

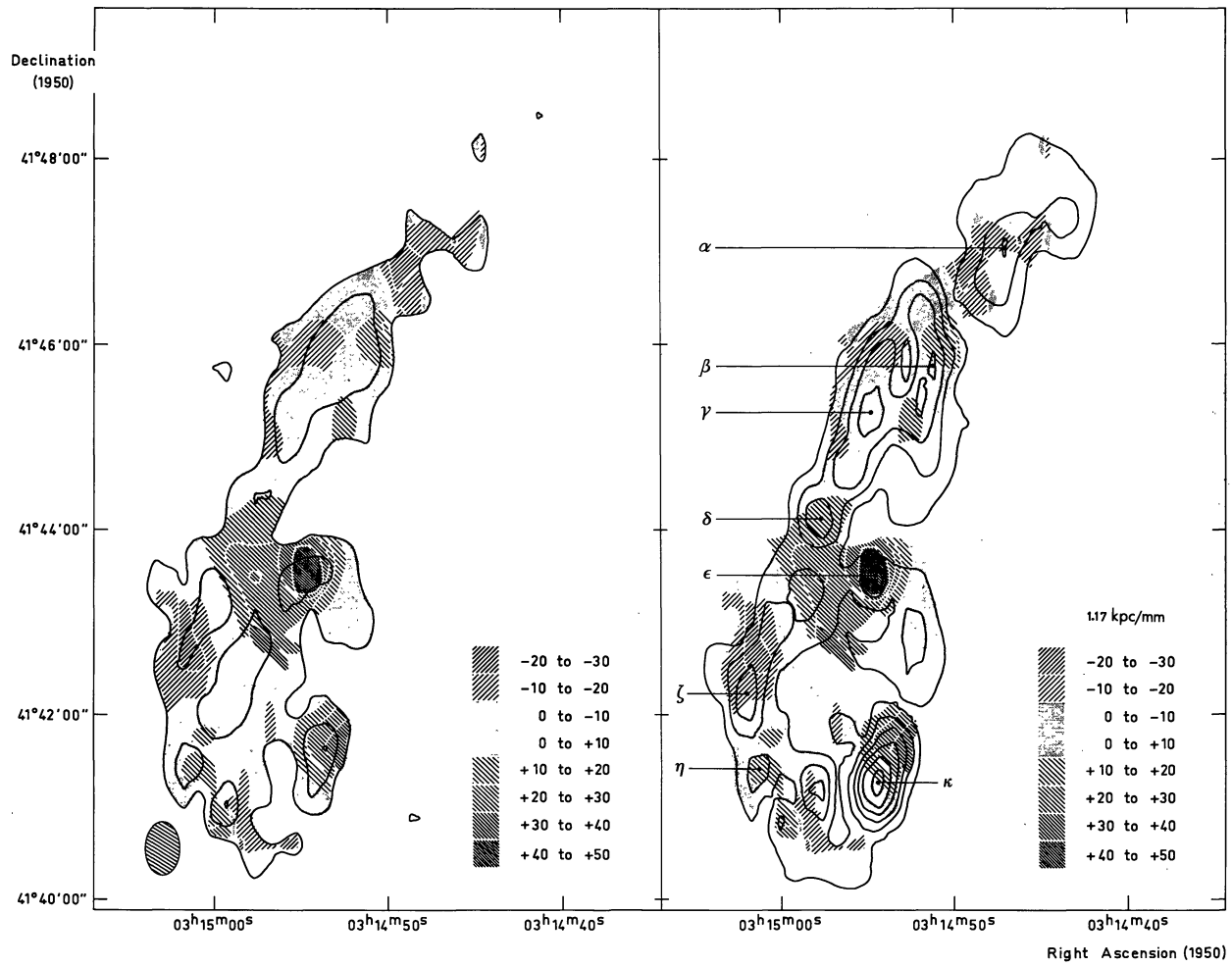

Fig. 5. The polarization intensity distribution of NGC 1265 at 5 GHz (left) and 1.4 GHz (right), both superimposed on a shaded map of the differential rotation measure distribution (see text). The rotation measure values are in rad m^{-2}. Contour levels of polarization are 3.5, 7 and 10.5 m.f.u. per synthesized beam at 5 GHz and at intervals of 5 m.f.u. between 5 and 30 m.f.u. at 1.4 GHz

of the 1.4 GHz total intensities (Miley, 1973) shows that the radiation is enhanced by about 10% at this position. These effects may well be due to a real constriction in the magnetic field lines. However we note the absence of a minimum in the 5 GHz polarized intensities. This wavelength dependence may indicate that instead we are seeing a twisting of the tail [as in 3 C 129 (Miley *et al.*, 1972)] with the two tail tubes crossing each other at this point. Such a superposition with opposite line-of-sight fields might result in reduced polarization at longer wavelengths together with a relatively small rotation measure.

6. Physical Conditions Inside and Outside the Source

6.1. Assumptions

To derive an illustrative set of values for the physical parameters characterizing the source we have made the following assumptions.

1. *The distance of* NGC *1265 (presumed in the Perseus Cluster) is* $D = 100$ Mpc.

This is equivalent to assuming a Hubble constant of 50 km s^{-1} Mpc^{-1}. Note that larger values of the Hubble constant have been used in most previous articles in this series.

2. *Each trail tube is a cylinder with an angular diameter of* $\phi = 23''$.

This is justified since the two sides of the tail are slightly resolved by our 23″ synthesized beam and there is no significant structure on a scale of 6″. For $D = 100$ Mpc, $\phi = 23''$ is equivalent to a linear size of ~ 10 Kpc.

3. *In the relativistic gas the heavy particle energy is equal to the electron energy* ($\xi = 1$).

4. *The radio spectrum of* 3 C *83.1* B *extends with single index from* 10^7 Hz *to* 10^{10} Hz.

5. *The direction of motion of* NGC *1265 makes an angle with the line of sight of* $i = 30°$.

The observed radial velocity v_r relative to the cluster mean is 2300 km s^{-1} (Chincarini and Rood, 1971). Since this lies on the outer wing of the velocity distribution for galaxies in the Perseus Cluster, the transverse velocity v_t is probably smaller. Also, the

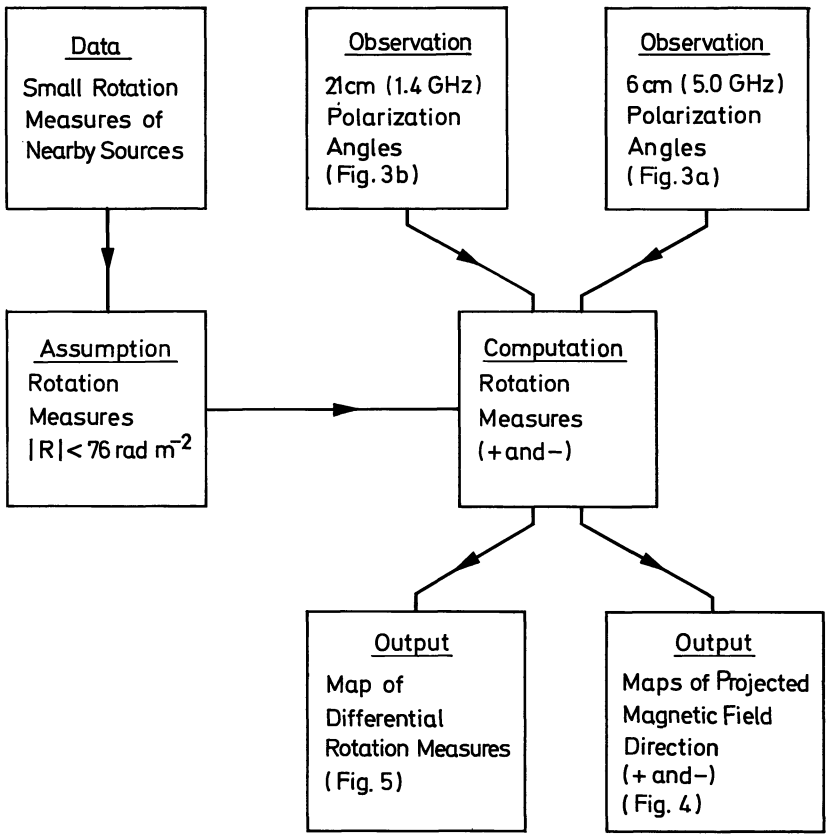

Fig. 6. Schematic diagram of the procedure used to derive the magnetic field and rotation measure distributions

Table 3

Position (Fig. 5)	Distance from galaxy (kpc)	Percentage polarization 5 GHz	1.4 GHz	Diff. rotation measure (rad m^{-2})	H_{eq} (μG)	n_e (10^{-4} cm^{-3})
α	205	(47)	44	−14	3.8	5.2
β	162	53	36	+12	4.3	4.0
γ	145	63	42	− 2	4.3	0.65
δ	106	30	34	+15	4.1	5.0
ε	87	23	12	+43	5.0	12.0
ζ	50	23	18	−17	4.9	4.9
η	26	(17)	(8)	+10	5.5	2.6
ϰ	21	(8)	13	+20	6.8	4.2

Because of the steep gradients in polarized intensities, values in brackets are subject to larger uncertainties.

linear extent of 3 C 83.1 B is only half that of the similar head tail source 3 C 129. Both points suggest that $20° < i < 40°$.

6. *Acceleration within the tail does not contribute substantially to the relativistic electron flux.*

In the usual double radio sources there is a well known conflict between the dynamic and the radiative lifetimes (e.g. van der Laan and Perola, 1969; Wardle and Miley, 1974). This problem is acute for the "hot spots" within the outer components of Cygnus A (Hargrave and Ryle, 1974). Spectral data indicate that the relativistic electrons responsible for the radiation at the hot spots are too young to have travelled there from the parent galaxy and *in situ* acceleration was invoked. In our case however, the smooth distributions of total intensity and magnetic field argue against any significant electron acceleration within the tail of 3 C 83.1 B. The intensity enhancement at the constriction mentioned earlier is a relatively small effect. If any appreciable *in situ* acceleration occurs it is almost certainly confined to the small components in the head.

7. *The map of differential rotation measure in Fig. 5 represents the distribution of intrinsic rotation measure in the source.*

See Section 4.

8. *Ejected component pairs are retarded with respect to the galaxy by ram pressure.*

9. *The tail is statically confined by thermal pressure.*

10. *The density of the external medium is constant around the source.*

Since the radio head lies within the optical contours of the galaxy (Wellington *et al.*, 1973) the density of the medium surrounding the head may well be larger.

6.2. *Internal Magnetic Fields*

For minimum total energy, the magnetic and particle energies are approximately equal (equipartition situa-

tion). The corresponding field strength (e.g. Pacholczyk, 1970) can be written as

$$H_{eq} \propto (1+\xi)^{2/7} C_{12}^{2/7} D^{-2/7} \phi^{-6/7} I_{1.4}^{2/7},$$

where $I_{1.4}$ is the 1.4 GHz radiation intensity and C_{12} can be evaluated numerically as a weakly dependent function of the spectral index α and the cut-off frequencies. Using $\alpha = -0.5$ and assumptions 1–4, H_{eq} was evaluated at several representative points in the source (see Fig. 5 and Table 3). Values obtained were in the range ~ 4 to $7\,\mu$G. If magnetic energy is dominant in the tail the real field strength H must be larger than these values.

Thus $H = \eta H_{eq}$ where $\eta > 1$.

We can obtain further information about H from the spectral data in Fig. 1, using reasoning similar to that applied to 3 C 129 by Jaffe and Perola. If (as implied by assumption 6) the spectral curvature is solely due to synchrotron and Compton losses, the radiative age of a point on the passive tail depends on the cut-off frequency ν^* and the magnetic field H. The dynamic age of that point can be derived using $v_r = 2300\ \mathrm{km\ s^{-1}}$ together with the distance and foreshortening factors from assumptions 1 and 5. Writing H_R for the microwave background's magnetic field we can relate H and ν^*, (e.g. van der Laan and Perola, 1969).

$$(D\theta\ \mathrm{cotan}\, i) \propto H^{1/2}(H^2 + H_R^2)^{-1} (\nu^*)^{-1/2},$$

where θ is the angular distance along the tail. Deriving ν^* from Fig. 1 and using assumptions 1 and 5 gives magnetic fields in the tail of $H \sim 3$–$7\,\mu$G. In view of the uncertainties these are not significantly different from H_{eq}. We therefore conclude that the magnetic field strengths cannot much exceed the equipartition values (i.e. $\eta \sim 1$) unless there is appreciable electron acceleration in the tail.

6.3. *Internal Densities*

We next obtain rough estimates for the densities n_e of thermal electrons within the source using values of the differential rotation measures from Fig. 5. Since the line of sight depth of a trail tube is $D\phi\ \mathrm{cosec}\, i$ we have

$$n_e \propto R H^{-1} (D\phi)^{-1} \tan i$$

hence

$$n_e \propto R \eta^{-1} \tan i (1+\xi)^{-2/7} C_{12}^{-2/7} D^{-5/7} \phi^{-1/7}.$$

Values of n_e for the points shown in Fig. 5 are listed in Table 3 and range from 10^{-3} to 10^{-2} electrons $\mathrm{cm^{-3}}$. They were calculated using $\eta = 1$ and assumptions 1–7. Their accuracy is limited mainly by our ignorance of the magnitude of foreshortening and of departures from equipartition.

The total mass of ionized gas in the tail, the product of the electron density and the volume, is

$$M \propto n_e D^3 \phi^2 \theta_0\ \mathrm{cosec}\, i$$

For $n_e \sim 10^{-3.7}$ and a total angular length of the tail θ_0 of 12′ we find $M \sim 5.10^8\ M_\odot$. This means a mass loss of $\sim 2\ M_\odot\ \mathrm{yr^{-1}}$.

Using the above values for H and n_e we also derive a formal value for the Alfvén speed in the tail: $V_A \sim 650\ \mathrm{km\ s^{-1}}$. This is less than a quarter of the speed of the galaxy with respect to the cluster.

6.4. *External Temperature and Density*

Finally let us use assumptions 8 to 10 to consider what constraints must be imposed on the *external* medium if it is to confine 3 C 83.1 B. We can obtain values for the external density ϱ_{ig} and temperature T_{ig} using the pressure balance arguments applied to 3 C 129 by Miley *et al.* (1972) and refined by Jaffe and Perola (1973).

First if we assume that the lagging frontal "blobs" in the head (Fig. 2) are dynamically retarded we can obtain a lower limit to ϱ_{ig}. Since the internal pressure in the blobs is equal to $H^2/8\pi$ we have

$$\varrho_{ig}(v_r \sec i)^2 > (\mathrm{const})\, \eta^2 (1+\xi)^{4/7} D^{-4/7} \psi^{-12/7} S_5^{4/7}, \qquad \text{(BLOB)}$$

where ψ is the angular diameter of a blob and S_5 its 5 GHz flux density. Since the blobs are unresolved we take $\psi < 6''$ and use assumptions 1, 3, 4 and 5. In the event of equipartition $\eta = 1$ and we then derive internal pressures $\sim 10^{-10}\ \mathrm{dyne\ cm^{-2}}$ and external densities $\sim 2.10^{-27}\ \mathrm{gm\ cm^{-3}}$ (i.e. $\sim 10^{-3}\ \mathrm{cm^{-3}}$). These are minimum values which will increase if equipartition is not satisfied.

Secondly, if the tail is thermally confined by a medium of the above density we can derive a value for the temperature:

$$T_{ig} \propto \varrho_{ig}^{-1} (1+\xi)^{4/7} D^{-4/7} \phi^{-12/7} I_{1.4}^{4/7}. \qquad \text{(TAIL)}$$

Substituting for ϱ_{ig} we find

$$T_{ig} < \frac{(v_r \sec i)^2}{(\mathrm{const})\, \eta^2} \left(\frac{\psi}{\phi}\right)^{12/7} \left(\frac{I_{1.4}}{S_5}\right)^{4/7}.$$

In this way we find that a temperature of $T_{ig} \sim 10^7$ K suffices to statically confine the passive part of the tail. We note however that if the density of the medium surrounding the head is larger (i.e. assumption 10 is invalid) a higher temperature T_{ig} would be required.

Independent information about the external temperature can be derived from the shape of the tail. Jaffe and Perola have shown that for the magnetospheric model the shape is related to the Mach number M_0 of the galaxy. In fact M_0 can be obtained from $\theta_c(\phi_c \sin i)^{-1}$ where ϕ_c is the ultimate angular diameter of the tail and θ_c is the angular distance from the nucleus at which this diameter is first attained. The speed of the galaxy

and the Mach number then allow an estimate of the sound speed in the medium and hence its temperature. Taking $\theta_c = \phi_c$ (from Fig. 2) and $i = 30°$ we find a sound speed of $\sim 700\,\mathrm{km\,s^{-1}}$ corresponding to an external temperature of $T_{ig} \sim 2.10^7$ K.

The values of external density and temperature are similar to those previously derived for the case of 3 C 129 and are consistent with a thermal bremsstrahlung interpretation for the X-ray emission of the Perseus Cluster (Gursky *et al.*, 1972; Kellogg and Murray, 1974).

7. Conclusions

The large polarization percentages and high degree of alignment of the polarization vectors show that the magnetic field in the tail of 3 C 83.1 B is remarkably uniform and *parallel* to the tail. This and all other observational data can be satisfactorily explained within the context of the magnetospheric model as follows: a dipole magnetic field in NGC 1265 is distorted by the motion of the galaxy through the cluster medium, forming a double hydromagnetic trail. The front of the trail is constricted by the high dynamic pressure; the trail progressively expands by a linear factor of ~ 3 until the internal pressure balances the external static pressure. The curved path of the trail is determined by the orbit of the galaxy through the cluster and by differential motions of the cluster medium. Intermittent outbursts in the nucleus of the galaxy produce relativistic particles that stream into the magnetic flux tubes of the trail. The particles diffuse along the magnetic field lines at the local Alfvén speed. This is much slower than the speed of the galaxy and the radio brightness is smoothed far from the receding particle source. Some particles are lost to the radio trail by diffusion into the ambient medium so that, even at low frequencies unaffected by energy losses, the brightness steadily decreases with increasing distance from the head. A major energy loss is radiative and the radio spectrum shows the ageing process. In this model the trail is clearly magnetohydrodynamically independent of the recurrent particle bursts that illuminate it.

The exact particle injection process is still an open question. In Section 6 we assumed (8) that pairs of relativistic plasmoids are ejected from the nucleus of NGC 1265. A plausible alternative is that the nucleus emits twin collimated relativistic beams of electrons similar to that proposed for the more usual double radio sources by Scheuer (1974) and Blandford and Rees (1974). It is not clear what the consequences would be if a collimated relativistic beam were emitted from a fast moving galaxy such as NGC 1265. The motion of the galaxy through the medium would at any rate prevent the formation of a large double source. When the beam impinges on the bow shock, the bulk motion might well be destroyed and the relativistic electrons would then diffuse down the magnetospheric trail with the Alfvén speed. The subsequent development would be described by the magnetospheric model. Investigation of the lagging frontal blobs in Fig. 2 is crucial to understanding the particle injection mechanism. Are the blobs ejected plasmoids or instabilities in a quasi-continuous flow of relativistic particles? Higher resolution measurements of the magnetic field distribution in the head could well decide between these alternatives.

Acknowledgements. We thank our many colleagues at Dwingeloo, Leiden and Westerbork without whom this article could not have been written.

The Westerbork Synthesis Radio Telescope is operated by the Netherlands Foundation for Radio Astronomy with the financial support of the Netherlands Organization for Pure Research (Z.W.O.).

References

Baars, J. W. M., van der Brugge, J. F., Casse, J. L., Hamaker, J. P., Sondaar, L. H., Visser, J. J., Wellington, K. J. 1973, *Proc. Inst. Elec. Electron. Engrs.* **61**, 1258

Blandford, R., Rees, M. 1974, *Monthly Notices Roy. Astron. Soc.* (in press)

Chincarini, G., Rood, H. J. 1971, *Astrophys. J.* **168**, 321

Gursky, H., Solinger, A., Kellog, E. M., Murray, S., Tananbaum, H., Giacconi, R., Cavaliere, A. 1972, *Astrophys. J.* **173**, L 99

Hargrave, P. J., Ryle, M. 1974, *Monthly Notices Roy. Astron. Soc.* **166**, 305

Heidmann, N. 1973, private communication

Hill, J. M., Longair, M. S. 1971, *Monthly Notices Roy. Astron. Soc.* **154**, 125

Högbom, J. A., Brouw, W. N. 1974, *Astron. & Astrophys.* **33**, 289

Jaffe, W. J., Perola, G. C. 1973, *Astron. & Astrophys.* **26**, 423

Kellogg, E., Murray, S. 1974, in preparation

Laan, H. van der, Perola, G. C. 1969, *Astron. & Astrophys.* **3**, 477

Miley, G. K. 1973, *Astron. & Astrophys.* **26**, 413

Miley, G. K., van der Laan, H., Wellington, K. J. 1973, IAU Symposium No. 58 (in press)

Miley, G. K., Perola, G. C., van der Kruit, P. C., van der Laan, H. 1972, *Nature* **237**, 269

Mitton, S. 1972, *Monthly Notices Roy. Astron. Soc.* **155**, 373

Pacholczyk, A. G. 1970, Radio Astrophysics, chapter 7, W. H. Freeman & Company, San Francisco

Riley, J. M. 1973, *Monthly Notices Roy. Astron. Soc.* **161**, 167

Ryle, M., Windram, M. D. 1968, *Monthly Notices Roy. Astron. Soc.* **138**, 1

Scheuer, P. A. G. 1974, *Monthly Notices Roy. Astron. Soc.* **166**, 513

Tifft, W. G. 1973, private communication

Vallée, J., Kronberg, P. K. 1974, in preparation

Wardle, J. F. C., Miley, G. K. 1974, *Astron. & Astrophys.* **30**, 305

Weiler, K. W. 1973, *Astron. & Astrophys.* **26**, 403

Weiler, K. W., Wilson, A. S. 1973, private communication

Wellington, K. J., Miley, G. K., van der Laan, H. 1973, *Nature* **244**, 502

G. K. Miley
H. van der Laan
Sterrewacht, Huygens Laboratorium
Wassenaarseweg 78
Leiden-2405, The Netherlands

K. J. Wellington
Division of Radiophysics, CSIRO
P.O. Box 76
Epping, N.S.W., 2121
Australia